



Shear strengthening of concrete members with TRM jackets: Effect of shear span-to-depth ratio, material and amount of external reinforcement

Zoi C. Tetta^{a,*}, Lampros N. Koutas^b, Dionysios A. Bournas^c

^a Dept. of Civil Engineering, University of Nottingham, NG7 2RD, Nottingham, UK

^b Dept. of Civil Engineering, University of Thessaly Volos, GR-38221 Greece

^c European Commission, Joint Research Centre (JRC), Directorate for Space, Security & Migration, Safety and Security of Buildings Unit, Via E. Fermi 2749, I-21027, Ispra, Italy

ARTICLE INFO

Keywords:

Carbon fibre
Glass fibres
Debonding
Fracture
Basalt fibres

ABSTRACT

An experimental work on reinforced concrete (RC) rectangular beams strengthened in shear with textile reinforced mortar (TRM) jackets is presented in this paper, with focus on the following investigated parameters: (a) the amount of external TRM reinforcement ratio, ρ_f , by means of using different number of textile layers and different types of textile fibre materials (carbon, glass, basalt); (b) the textile geometry, and (c) the shear span-to-depth ratio, a/d . In total, 22 tests were conducted on simply supported rectangular RC beams under (three-point bending) monotonic loading. The experimental results revealed that: (1) TRM is very effective when the failure is attributed to debonding of the TRM jacket from the concrete substrate; (2) the trend of effective strains for carbon, glass and basalt TRM jackets is descending for increasing values of the TRM reinforcement ratio, ρ_f , when failure is associated to debonding of the jacket; (3) the effect of textile geometry is significant only for low values of ρ_f , resulting in variances in the capacity enhancement and the failure modes, and (4) the shear span-to-depth ratio has practically no effect to the failure mode nor to the TRM jacket contribution to the total shear resistance of the RC beams.

1. Introduction and background

Over the last decades, there is an increasing need to upgrade many of the existing RC structures both in seismic and non-seismic areas mainly due to their ageing, lack of maintenance, deterioration, and environmental induced degradation.

A composite material called textile-reinforced mortar (TRM) has been introduced since last decade, for structural strengthening of existing structures [1,2]. TRM consists of textile fibre reinforcement (with open-mesh configuration) combined with inorganic matrices (i.e. cementitious mortars). The acronym 'FRCM' is also used in the literature for the same material [3]. TRM is a low-cost, resistant at high temperature [4–6], compatible to masonry or concrete substrates and friendly for manual workers material, which can be applied at low temperatures or on wet surfaces. Therefore, the use of TRM is becoming more attractive for the retrofitting of existing concrete or masonry structures than fiber-reinforced polymers (FRP) which have been widely used but has some drawbacks (i.e. high prices, inapplicability at low temperatures or wet surfaces, combustibility that could boost fire spreading and generally very poor performance at high temperature) due to the epoxy resins used in these composites. Bond between TRM or

FRCM and concrete substrates has been widely studied in the last decade [i.e. 5, 7–8]. TRM has also been studied for flexural strengthening [i.e. 9–14], torsional strengthening [15], confinement, seismic retrofitting of RC elements [16–19], repairing of corroded T-beams [20], strengthening of masonry elements [21–26] has been found to be a very promising solution. Examples of real applications of TRM system are presented in Ref. [27]. A variety of studies on TRM have been published the last year (2017), indicating that TRM is on the spotlight of recent research [28–41].

The assessment of existing RC structures with the existing standards (i.e. Eurocodes) often results in shear deficient beams or bridge girders due to corrosion of the shear links, low concrete strength or/and increased applied loads. A number of studies have investigated the use of TRM jacketing for shear strengthening of RC beams [1,42–53]. In these studies the main investigated parameters were the performance of TRM versus FRP jackets [1,46,48,52,53], the number of layers [1,42,44,46,48,51,52], the strengthening configuration [45,48], the anchorage of TRM U-shaped jackets in T-beams [22,44,52] and the amount of internal shear reinforcement [53].

In particular, Tzoura and Triantafyllou [46] reported that FRP jackets (that failed due to debonding of the jacket) were much more

* Corresponding author.

E-mail addresses: zoi_tetta@hotmail.com (Z.C. Tetta), koutasciv@gmail.com (L.N. Koutas), dionysios.bournas@ec.europa.eu (D.A. Bournas).

effective than their counterparts TRM jackets which failed due to slippage of fibres through the mortar. In contrast, Tetta et al. [48], Tetta et al. [52] and Awani et al. [53] concluded that TRM U-shaped jackets are practically as effective as equivalent FRP U-shaped jackets due to the common failure mode which was debonding of the jacket from the concrete substrate. Shear capacity is considerably increased by increasing the number of layers [46,48,52,53]. Azam and Soudki [45] reported that the strengthening configuration, namely side-bonded or U-shaped jackets did not affect the performance of TRM jacketing, whereas Tetta et al. [48] concluded that side-bonded jackets are much less effective than U-shaped jackets in increasing the shear resistance of concrete beams. Bruckner et al. [44] and Tzoura and Triantafillou [46] investigated the use of mechanical end-anchorage system in shear strengthening of T-beams with carbon or glass U-shaped TRM jackets, concluding that the early debonding of the TRM jacketing can be delayed using metallic anchors and therefore the effectiveness of the TRM jackets can be considerably improved. However, metallic anchors are susceptible to corrosion and their use is often related with tearing of the composite materials due to concentration of stresses. Therefore, Tetta et al. [52] very recently applied a novel end-anchorage system in U-shaped jackets using textile-based anchors and increased substantially the effectiveness of TRM jackets. Also very recently, Awani et al. [53] reported that the gain in shear capacity decreased with the increase in the amount of stirrups. In one of the latest studies, Tetta and Bournas [4] compared TRM with FRP jackets for strengthening in shear concrete beams subjected to high temperature. They concluded that both two-sided and U-shaped TRM jackets are considerably more effective than their counterparts FRP jackets when specimens are exposed to high temperature (100 °C and 150 °C).

The past studies on shear strengthening of concrete beams with TRM led to interesting conclusions about the effectiveness of the technique, however from the literature review presented above, it is clear that the use of TRM for shear strengthening of concrete beams has not been sufficiently investigated yet. This study presents for the first time in a systematic way the effect of the external reinforcement ratio (ρ_f) in three different textile materials, namely carbon, glass and basalt investigating at least three different values of external reinforcement ratio (ρ_f) for each textile material. Moreover, this study investigates for the very first time the effect of the shear span-to-depth ratio, a/d ($a/d = 1.6, 2.6$ and 3.6) on concrete beams strengthened in shear with U-shaped TRM jackets. The following sections provide all the details.

2. Experimental program

2.1. Specimens and experimental parameters

A total of 22 RC beams (102×203 mm) were constructed and tested as simply supported under three-point bending monotonic load. Specimens had total length and effective flexural span equal to 1677 mm and 1077 mm, respectively (Fig. 1a). Three different shear span-to-depth ratios, namely $a/d = 1.6, 2.6$ and 3.6 were studied. The beams were intentionally designed as shear deficient in one of the two shear spans. Therefore, one shear span did not include any stirrups, whereas the other shear span included stirrups of 8 mm diameter at a spacing of 100 mm, 75 mm and 50 mm at the beams of shear span ratio, a/d equal to 1.6, 2.6 and 3.6, respectively (Fig. 1a).

TRM jacketing was applied at the shear span without stirrups, in order to increase its shear capacity. The beams were designed such the shear force corresponding to the flexural resistance of the beams were 3 times the shear capacity of the unretrofitted beam. Two deformed bars of 16 and 10 mm diameter, respectively, were used as tensile and compressive longitudinal reinforcement of the beams, as shown in Fig. 1b. The tensile reinforcement ratio was 2.2% and the effective

depth of the beams was equal to 177 mm. The main experimental parameters in this paper are:

- the effect of the amount of external TRM reinforcement ratio, ρ_f , using different textile materials (carbon, glass and basalt)
- the textile geometry
- the shear span-to-depth ratio, a/d .

Three beams with shear span-to-depth ratios equal to 1.6 (CON_1.6), 2.6 (CON) and 3.6 (CON_3.6) were used as control specimens and tested, whereas the rest of the specimens were strengthened by U-shaped TRM jackets. Four different textile grids were used, two carbon (a light and a heavy-weight carbon textile), a glass and a basalt fibre textile.

The details of the specimens are presented in Table 1. Fig. 2 depicts all the strengthening schemes adopted in retrofitted specimens. The notation of strengthened specimens is Y1L1_Y2L2, where Y1 and Y2 denote the first and second (if any) textile reinforcement, respectively, and L1, L2 denote the number of TRM layers of the first and second (if any) textile reinforcement (CL for light-weight carbon, CH for heavy-weight carbon, G for glass and B for basalt), respectively. The suffix 'strips' was used for specimen strengthened with strips that were combined with continuous TRM layer. For beams with a/d different than 2.6, a suffix with the shear span-to-depth ratio (1.6 or 3.6) was used. The description of the retrofitted beams follows:

- CL1 and CL3: beams with $a/d = 2.6$, strengthened with 1 and 3 light carbon TRM layers, respectively.
- CH1_CL1, CH2_CL1 and CH3_CL1: beams with $a/d = 2.6$, that strengthened with 1 light carbon TRM layer combined with 1, 2 and 3 heavy-weight carbon TRM layers, respectively.
- CL1_strips: beam with $a/d = 2.6$, that strengthened with 1 light carbon TRM layer combined with light carbon strips of 125 mm width, as shown in Fig. 2.
- G1, G3 and G7: beams with $a/d = 2.6$, strengthened with 1, 3 and 7 glass TRM layers, respectively.
- B1, B3 and B7: beams with $a/d = 2.6$, strengthened with 1, 3 and 7 basalt TRM layers, respectively.
- CL1_1.6 and CL3_1.6: beams with $a/d = 1.6$, strengthened with 1 and 3 light carbon TRM layers, respectively.
- CL1_3.6 and CL3_3.6: beams with $a/d = 3.6$, strengthened with 1 and 3 light carbon TRM layers, respectively.

2.2. Materials and strengthening procedure

Casting of specimens was made by using the same concrete. The concrete compressive strength and the concrete tensile splitting strength were obtained by testing concrete cylinders (300×150 mm) on the day of testing the beams. Table 1 summarizes the (average of 3 specimens) concrete strength values. The yield stress (average of 3 specimens) of longitudinal bars with 16 and 10 mm diameter was equal to 547 MPa and 552 MPa, respectively, whereas the yield stress of the steel bars with 8 mm diameter used for stirrups, was equal to 568 MPa.

The four textile grid materials used in this study have equal amount of fibres in two orthogonal directions. The weight of the light carbon, heavy carbon and glass textiles was equal to 220 g/m², 348 g/m² and 220 g/m², respectively, whereas the weight of basalt textile including 10% coating was 220 g/m². The nominal thickness, t_f (based on the equivalent smeared distribution of fibres) of the light carbon, heavy carbon, glass and basalt textile was 0.062 mm, 0.095 mm, 0.044 mm and 0.037 mm, respectively as shown in Fig. 3. The modulus of elasticity of the fibres, E_f , for each textile, is included in both Fig. 3 and Table 1.

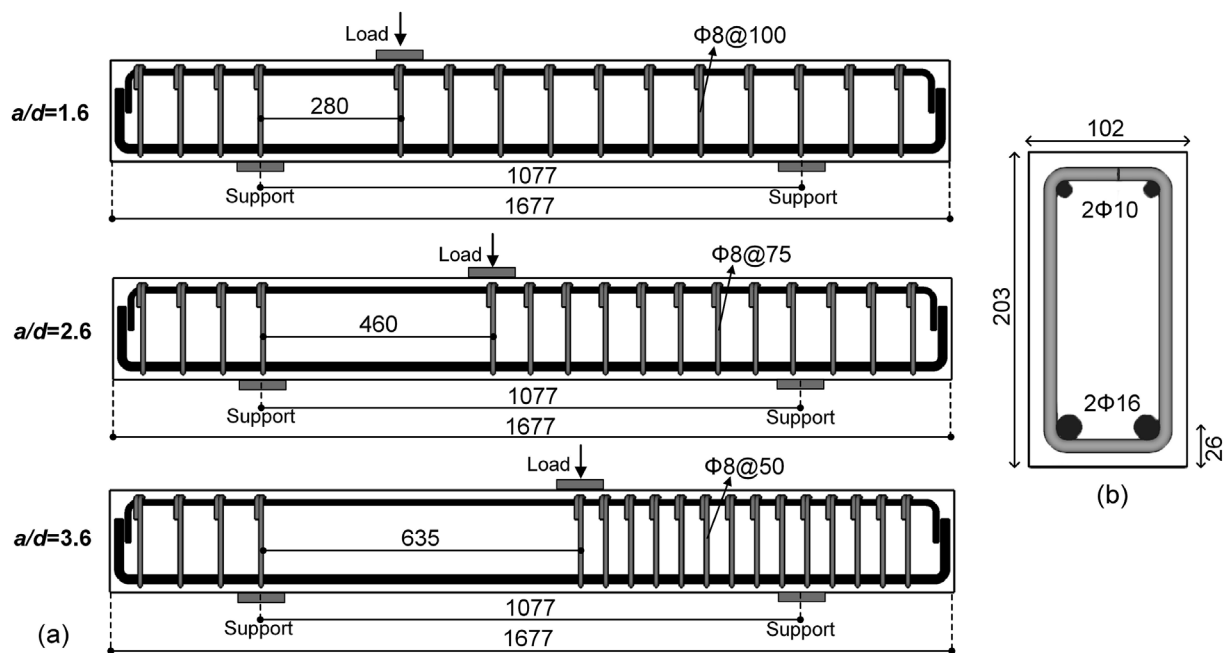


Fig. 1. (a) Schematic test set-up; (b) cross-section (dimensions in mm).

Table 1
Strengthening configuration and material properties of all specimens.

Specimen	ρ_f (%)	E_f (GPa)	$E_{f,TRM}$ (GPa)	$\rho_f E_{f,TRM}$ (MPa)	Concrete strength (MPa)		Mortar strength (MPa)		
					Compressive strength	Tensile splitting strength	Compressive strength	Flexural strength	
a/d = 2.6									
CON ^a	–	–	–	–	21.6	2.36	–	–	
CL1	1.2	225	167.6	203.75	23.0	2.50	38.7	9.10	
CL1_strips	1.9	225	167.6	312.20	20.0	1.98	38.7	9.10	
CH1 ^b	1.9	225	163.3	304.19	23.8	2.73	31.1	10.3	
CH1_CL1 ^c	3.1	225	165.5	507.94	20.0	1.98	38.7	9.10	
CH2 ^a	3.7	225	163.3	608.37	23.8	2.73	31.1	10.3	
CL3 ^b	3.6	225	167.6	611.25	20.8	2.39	35.5	8.10	
CH2_CL1 ^c	4.9	225	164.7	812.12	20.0	1.98	38.7	9.10	
CH3 ^a	5.6	225	163.3	912.56	22.6	2.81	26.9	8.64	
CH3_CL1 ^c	6.8	225	164.4	1116.31	20.0	1.98	38.7	9.10	
G1	0.9	74	41.1	35.46	20.0	1.98	35.5	8.10	
G3	2.6	74	41.1	106.38	20.0	1.98	35.5	8.10	
G7 ^b	6.0	74	41.1	248.21	20.0	1.98	38.7	9.10	
B1	0.7	89	63.7	46.34	23.1	2.48	33.3	11.05	
B3	2.2	89	63.7	139.02	23.1	2.48	35.5	8.10	
B7	5.1	89	63.7	324.37	23.1	2.48	35.5	8.10	
a/d = 1.6									
CON_1.6	–	–	–	–	20.5	2.35	–	–	
CL1_1.6	1.2	225	167.6	203.75	22.6	1.95	33.3	11.05	
CL3_1.6	3.6	225	167.6	611.25	22.6	1.95	33.3	11.05	
a/d = 3.6									
CON_3.6	–	–	–	–	20.5	2.35	–	–	
CL1_3.6	1.2	225	167.6	203.75	22.6	1.95	33.3	11.05	
CL3_3.6	3.6	225	167.6	611.25	22.6	1.95	33.3	11.05	

^a Specimens included in Tetta et al. 2015 [28].

^b Specimens included in Tetta and Bournas 2016 [4].

^c $\rho_f E_{f,TRM} = \rho_{f,CH} E_{f,TRM,CH} + \rho_{f,CL} E_{f,TRM,CL}$.

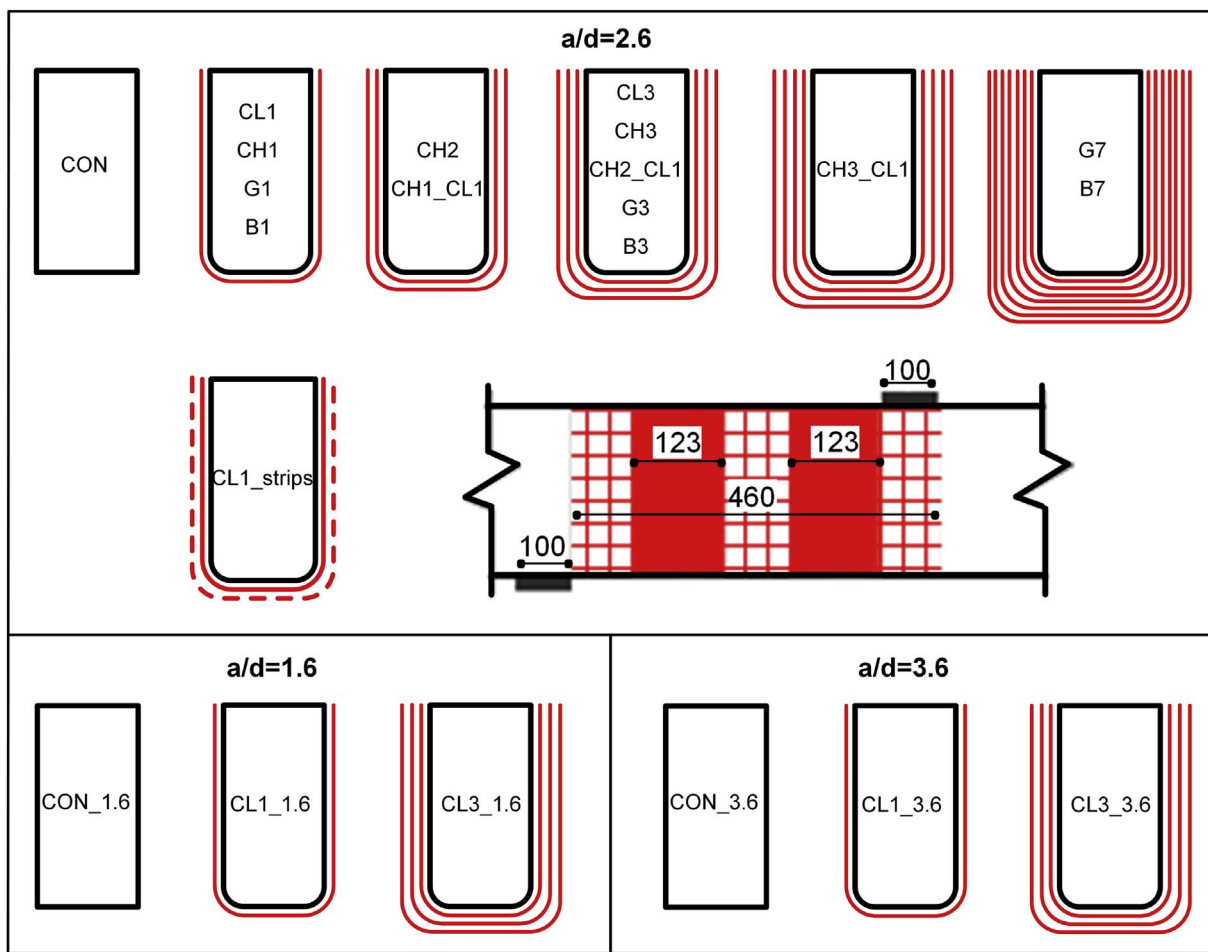


Fig. 2. Schematic representation of different strengthening configurations.

A polymer-modified cementitious mortar was used as matrix of the TRM composite material which was the same for all four textile materials. The cement-to-polymers ratio was equal to 8:1, whereas the water-to-cement ratio was equal to 0.23. The strength properties (average values of 3 specimens) of the mortar experimentally obtained

through prisms on the day of testing according to the EN 1015-11 [54] are summarized in Table 1.

As shown in Fig. 4a, before the application of TRM jacketing, the concrete surface was properly prepared by grinding the concrete surface and creating a grid grooves. To avoid stress concentration, the two

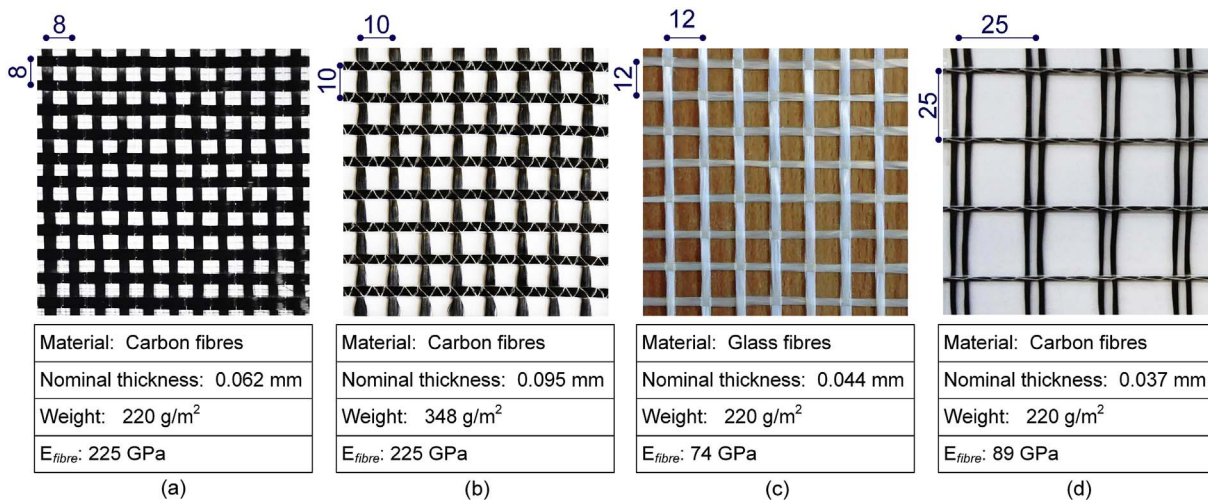


Fig. 3. Textiles used in this study: (a) light carbon-fiber textile; (b) heavy carbon-fiber textile; (c) glass-fiber textile; (d) basalt-fiber textile (dimensions in mm).

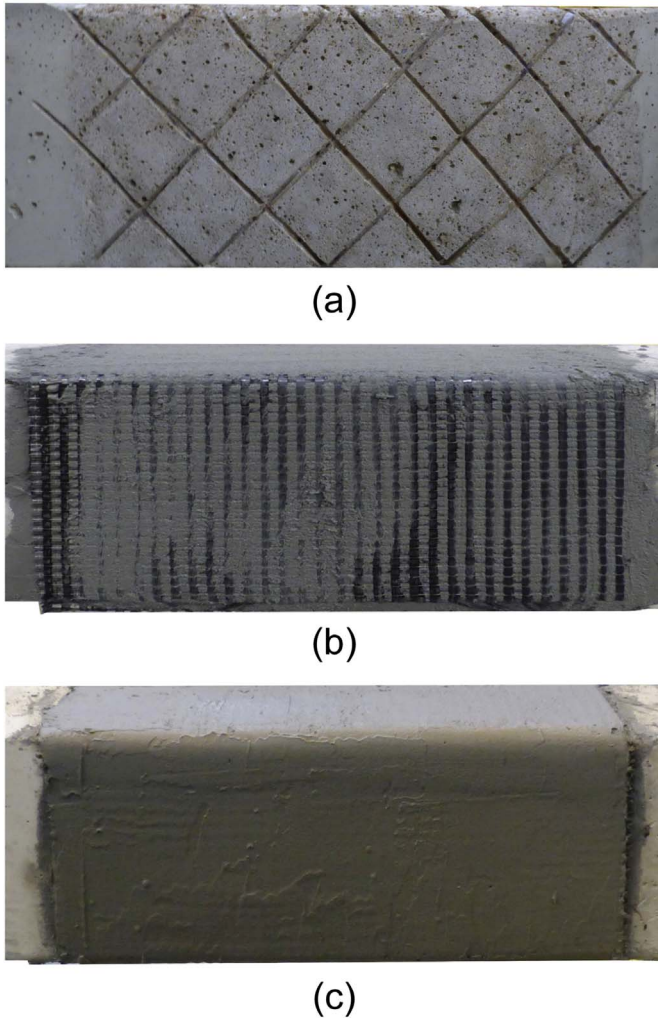


Fig. 4. (a) Prepared concrete surface before strengthening; (b) impregnation of the textile fibres with mortar; (c) final layer of mortar on the top of the final textile layer.

bottom edges of each specimens were rounded (radius equal to 15 mm). The first 2 mm-thick mortar layer was applied on the (dampened) concrete surface by using a smooth metal trowel. The first layer of textile was applied after the application of the first mortar layer and then pressed slightly into the mortar by hand pressure to fully immerse the fibre roving (Fig. 4b). A layer of mortar was then applied to completely cover the textile. The rest textile layers were applied by following the aforementioned procedure (Fig. 4c). It is very important in this method to apply each layer of mortar while the previous layer is still fresh.

2.3. Tensile tests in TRM coupons

Three (dumbbell) tensile coupons for each textile mesh material with the geometry shown in Fig. 5a were prepared and tested at a monotonic displacement rate of 0.02 mm/s to characterise the tensile behaviour of the composite material. A universal testing machine of 200 kN load-capacity was used for conducting the uniaxial tensile testing. Two LVDTs were attached on the coupon (one on each side) to measure its axial deformation (Fig. 5b). The response of all TRM coupons comprised three distinct stages:

- (1) the specimen remains uncracked
- (2) development of multiple cracks after the first cracking occurs
- (3) the cracking pattern has fully developed and the increase in resistance is due to the textile itself until rupture of fibres is observed.

Table 2 includes the mean values of ultimate tensile stress (f_{fu}), ultimate tensile strain (ϵ_{fu}) and the modulus of elasticity at the cracked stage, $E_{f,TRM}$ that is the secant modulus of elasticity of the 3rd branch of the stress-strain curve. The modulus of elasticity of the TRM jacket, $E_{f,TRM}$, for each beam is also included in Table 1.

2.4. Experimental setup and procedure

As shown in Fig. 6, the beams were tested under three-point bending monotonic loading at a displacement rate of 0.02 mm/s using a stiff steel reaction frame. The load was applied using a 500 kN-capacity servo-hydraulic actuator that was vertically positioned. An external LVDT was used to measure the vertical displacement at the load application position as illustrated in Fig. 6; the displacement measurements from this LVDT was used in load versus displacement curves, presented in Section 3. Moreover, the Digital Image Correlation (DIC) method was also used to monitor the field of displacements within strengthening zone, using two high-resolution cameras.

3. Experimental results

The load versus displacement curves of all beams with $a/d = 2.6$ strengthened with carbon, glass and basalt TRM jackets are presented in Fig. 7a–c, respectively, whereas the shear force versus displacements curves of the beams with different a/d ratios are included in Fig. 8a–c. Table 3 includes:

- (a) The ultimate load
- (b) the displacement corresponding at the ultimate load
- (c) the observed failure mode
- (d) V_R , which is the shear resistance of the critical shear span
- (e) the contribution of the TRM jacket to the shear resistance of the beam, V_f
- (f) The increase in the shear capacity owing to TRM jacketing, $V_f/V_{R,con}$ (%)
- (g) the effective strain of the TRM jacket, ϵ_{eff} (%) which is defined using the following equation:

$$\epsilon_{eff} = V_f / (\rho_f E_{f,TRM} b_w 0.9d) \quad (1)$$

It is worth mentioning that the calculation of V_f values and therefore ϵ_{eff} values has been based on the simplified hypothesis that the two mechanisms of carrying forces (concrete contribution and jacket contribution) are superimposed without considering any interaction between them. The interaction between mechanisms of carrying forces is more pronounced when stirrups are used [55,56].

The control beam with $a/d = 2.6$ (CON) failed in shear at a peak load of 51.8 kN, when a large shear crack opened in the critical shear span. (Fig. 7a).

Specimens CH1 and CH2 reached an ultimate load of 78.2 and 120.2 kN, respectively, resulting in 50.8% and 132% shear capacity increase. Failure of specimen CH1 was due to slippage of the fibre rovings through the mortar and rupture of the fibres at the outer layer of the roving along the shear crack (Fig. 9a). In specimen CH2 the TRM jacket was debonded with part of concrete at a large area of the critical shear span (Fig. 9b).

Specimens CL1, CL1_strips, CH1_CL1, CL3, CH2_CL1, CH3 and

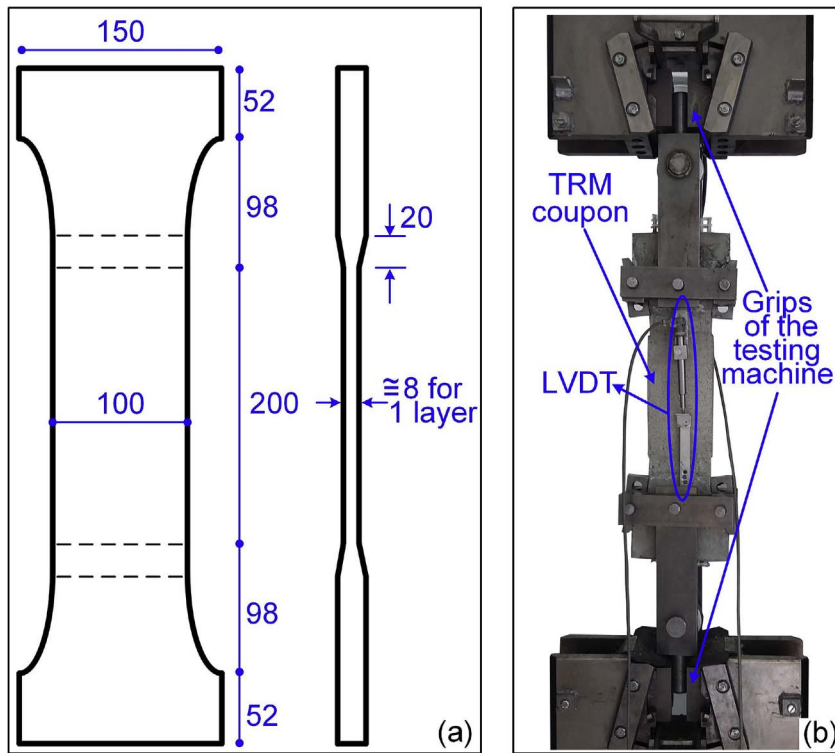


Fig. 5. Three-point bending test set-up of beams.

Table 2
Summary of TRM coupons results.

	Light-weight Carbon Textile (CL) ^a	Heavy-weight Carbon Textile (CH) ^a	Glass textile (G) ^a	Basalt textile (B) ^a
Tensile strength, f_{tu} (MPa)	1501 (132)	1382 (115)	794 (86)	1188 (127)
Ultimate tensile strain, ϵ_{fu} (%)	0.79 (0.095)	0.79 (0.069)	1.66 (0.13)	1.83 (0.11)
Modulus of elasticity of cracked specimen, $E_{f,TRM}$ (GPa)	167.6 (21)	163.3 (16)	41.1 (5)	63.7 (8)

^a Standard deviation in parenthesis.

CH3_CL1 failed in shear at a peak load 102.3, 110.7, 117.4, 118, 129.3, 131.1 and 136.5 kN, respectively, which yields 97.3%, 113.5%, 132%, 127.6%, 149.5%, 152.9% and 163.3% shear capacity increase, respectively. In all these beams TRM jacket was debonded from the concrete substrate at the full-length of the shear span with part of the concrete cover (Fig. 9c–i).

The peak load attained by specimens G1, G3, G7, B1, B3 and B7 was 73.2, 117.3, 144.3, 76.9, 114.9 and 135.4 kN, respectively, which yields 41.1%, 124.6%, 178.5%, 48.5%, 121.5% and 161.3% increase in the shear capacity, respectively. Failure of specimens G1 and B1 was due to fracture of the textile fibres crossing the shear crack (Fig. 10a and d), whereas in specimens G3, G7, B3 and B7 TRM jacket was debonded with part of the concrete cover (Fig. 10b–c, e–f).

The control beams with $a/d = 1.6$ and with $a/d = 3.6$ failed in shear at an ultimate load of 88.4 and 62.2 kN, respectively. In specimen CON_3.6 a large shear crack was formed at the critical shear span

(Fig. 11a) similar to the control specimen with $a/d = 2.6$. On the contrary, specimen CON_1.6, with the smallest shear-span-to depth ratio, failed in shear compression (Fig. 11b). Finally, specimens CL1_1.6, CL3_1.6, CL1_3.6 and CL3_3.6 reached an ultimate load of 123.7, 142.7, 133.8 and 158.7 kN, respectively, resulting in 39.9%, 61.5%, 115.3% and 155.3% shear capacity increase, respectively. These specimens failed in the same way with their counterpart specimens with $a/d = 2.6$, namely full detachment of the jacket from the substrate including part of the concrete cover. In specimen CL1_3.6, the debonding was initiated at the load application position and progressed towards the area below the shear crack (Fig. 11c), whereas in specimens CL1_1.6, CL3_3.6 and CL3_1.6, the TRM jackets debonded at the full-length of the shear span as shown in Fig. 11d–f, respectively.

4. Discussion

All beams failed in shear as designed and therefore the capacity of all retrofitting configurations in increasing the shear resistance of the beams was successfully evaluated. The results of this experimental programme were examined in terms of shear capacity increase and failure modes observed, revealing the following information for the various parameters investigated in this study.

4.1. Effect of external reinforcement ratio and axial rigidity

Fig. 12a–b plots the experimentally obtained effective strains, ϵ_{eff} , against the ρ_f and $\rho_f E_{f,TRM}$ values, respectively ($\rho_f E_{f,TRM}$ values represent the axial rigidity of the strengthening layers (that constitutes an important parameter [57,58]), because the width of all beams is the same) for the beams retrofitted with carbon-fibre TRM jackets. Results from three FRP-retrofitted beams presented in Refs. [4,42] (having identical geometry with the beams tested here), are also included in the

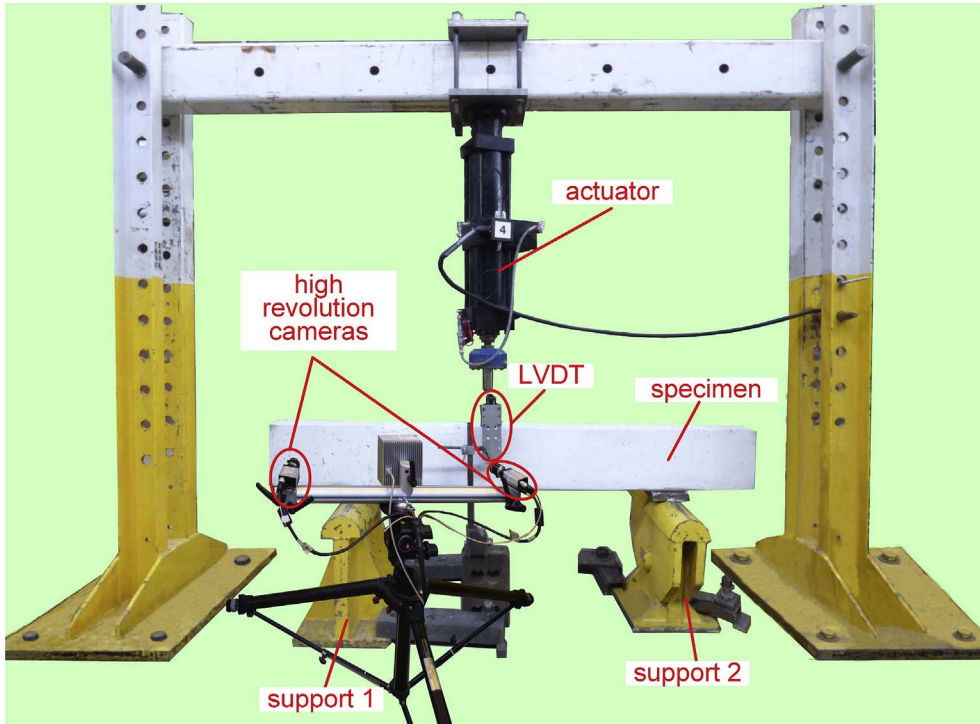


Fig. 6. (a) Geometry of TRM coupons; (b) test set-up for tensile testing of TRM coupons; (c) stress versus strain curves.

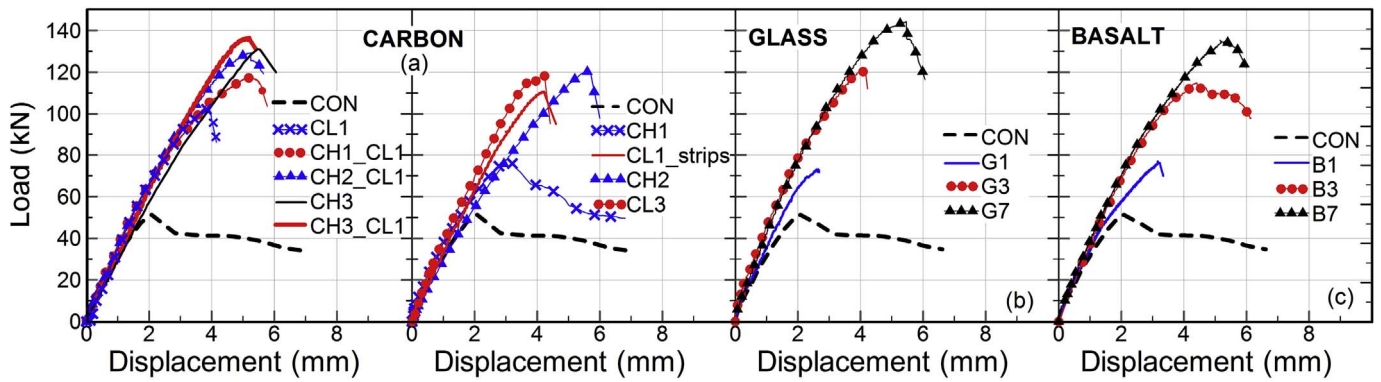


Fig. 7. Load versus vertical displacement curves for all tested specimens of 2.6 shear span-to-depth ratio.

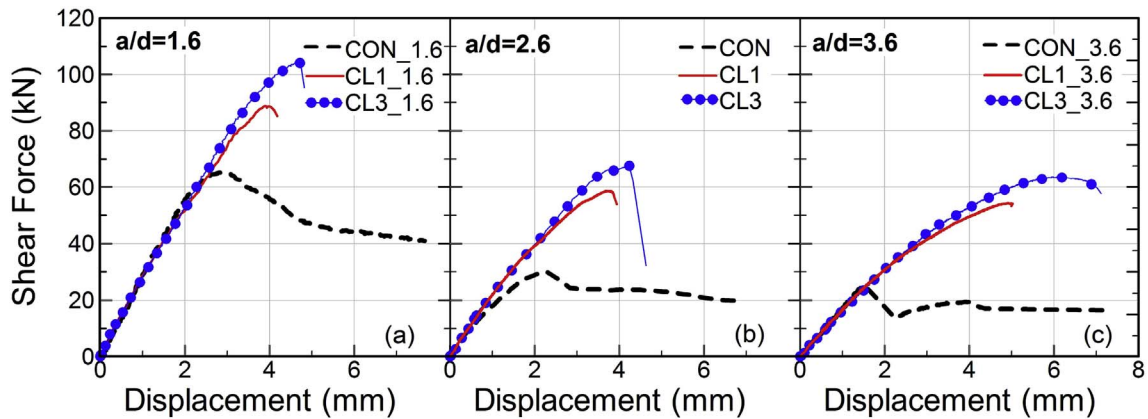


Fig. 8. Shear force versus vertical displacement curves for all tested specimens of shear span-to-depth ratio equal to 1.6, 2.6 and 3.6.

Table 3
Summary of test results.

Specimen	(a) Peak load (kN)	(b) Displacement at peak load (mm)	(c) Failure mode	(d) V_R (kN)	(e) V_f (kN)	(f) Shear capacity increase $V_f/V_{R,con}$ (%)	(g) ϵ_{eff} (‰)
$a/d = 2.6$							
CON	51.8	2.27	Tensile diagonal shear	29.7	–	–	–
CL1	102.3	3.77	D	58.6	28.9	97.3	8.73
CL1_strips	110.7	4.22	D	63.4	33.7	113.5	6.64
CH1	78.2	3.09	S	44.8	15.1	50.8	3.06
CH1_CL1	117.4	5.19	D	67.3	37.6	126.6	4.54
CH2	120.2	5.60	D	68.9	39.2	132.0	3.97
CL3	118	4.38	D	67.6	37.9	127.6	3.82
CH2_CL1	129.3	5.24	S	74.1	44.4	149.5	3.36
CH3	131.1	5.47	D	75.1	45.4	152.9	3.06
CH3_CL1	136.5	5.20	D	78.2	48.5	163.3	2.67
G1	73.2	2.59	FR	41.9	12.2	41.1	21.17
G3	117.3	4.09	D	67.2	37.0	124.6	21.41
G7	144.3	5.47	D	82.7	53	178.5	13.14
B1	76.9	3.16	FR	44.1	14.4	48.5	19.13
B3	114.9	4.38	D	65.8	36.1	121.5	15.98
B7	135.4	5.15	D	77.6	47.9	161.3	9.09
$a/d = 1.6$							
CON_1.6	88.4	2.93	Shear compression	65.4	–	–	–
CL1_1.6	123.7	3.85	D	91.5	26.1	39.9	7.88
CL3_1.6	142.7	4.66	D	105.6	40.2	61.5	4.05
$a/d = 3.6$							
CON_3.6	62.2	1.51	Tensile diagonal shear	25.5	–	–	–
CL1_3.6	133.8	4.91	D	54.9	29.4	115.3	8.88
CL3_3.6	158.7	5.92	D	65.1	39.6	155.3	3.99

D for debonding, S for slippage of the vertical fibre rovings through the mortar and partial fibres rupture, FR for Fracture of the jacket.

plot of Fig. 12a–b for comparisons. Also Table 4 includes all the important results of the three FRP-strengthened beams, presented in Refs. [4,48]. From the comparison in Fig. 12a–b, it becomes evident that TRM is as effective as FRP jacketing in increasing the shear capacity of concrete beams, when failure is associated to debonding of the jacket. In specific, for this type of failure the trend of the experimental ϵ_{eff} values for TRM jackets is descending for increasing $\rho_f E_{f,TRM}$ values, which is in agreement with the typical behaviour of FRP jackets. As also shown in Fig. 12b, TRM consisting of heavy-carbon fibre textile is less effective than equivalent FRP system (in terms of $\rho_f E_{f,TRM}$) or TRM consisting of light-carbon fiber textile, when premature failure due to slippage of fibres occurs.

Fig. 12c–d plots the experimental effective strains versus, ϵ_{eff} , against the ρ_f and $\rho_f E_{f,TRM}$ values, respectively for beams strengthened with glass and basalt TRM U-shaped jackets. In case of low $\rho_f E_{f,TRM}$ values ($\rho_f E_{f,TRM} < 100$ MPa), failure of specimens is associated with the rupture of the fibres (basalt or glass) in the TRM jackets, resulting in full exploitation of the tensile capacity of the textiles. Increasing the $\rho_f E_{f,TRM}$ values, debonding failure was experienced (TRM jacket was debonded with part of concrete cover). As in the case of carbon textiles, the trend of the experimental ϵ_{eff} values for glass and basalt TRM jackets is also descending for increasing ρ_f values, when debonding of the jacket was experienced.

4.2. Effect of textile geometry

In this section the effect of the geometry of the textile fibre material

on the failure mode and performance of TRM jackets is studied. The effect of the textile geometry on the behaviour of specimens strengthened with equivalent (in terms of ρ_f) carbon TRM jackets is first discussed, whereas the effect on the failure mode of beams strengthened with one TRM layer of different textile material (carbon, glass and basalt) follows next.

Specimens CL1_strips and CH1 had the same reinforcement ratio (equal to 1.9‰), comprising TRM jackets with carbon textiles of different geometry (see Fig. 2). Following the same concept, specimens CL3 and CH2 strengthened with correspondingly 3 and 2 layers of light and heavy carbon textile, having the same reinforcement ratio ($\rho_f \approx 3.6$ ‰). Fig. 13a and b depicts the mesh pattern of both heavy and light carbon fibre textiles, respectively. It can be observed that the combination of wider rovings (4 mm) with smaller mesh size (8 mm) in the light carbon textile (Fig. 13b), allows for a denser mesh-pattern when compared to the heavy carbon textile with 3 mm-wide rovings and 10 mm-mesh.

By comparing the results of specimens CH1 and CL1_strips, it is shown that the geometry of the textile fibre material has a strong effect on the failure mode and as a result on the shear capacity of beams in case of low external reinforcement ratio ($\rho_f \approx 1.9$ ‰). As mentioned in Section 3, specimen CH1 failed due to slippage of fibres through the mortar and rupture of fibres at the outer layer of roving along the shear crack contrary to the failure of specimen CL1_strips that was attributed to debonding of the TRM jacket with part of concrete cover. The increase in shear capacity of specimens CH1 and CL1_strips, was 50.8% and 113.5%, respectively, whereas the effective strains for specimens

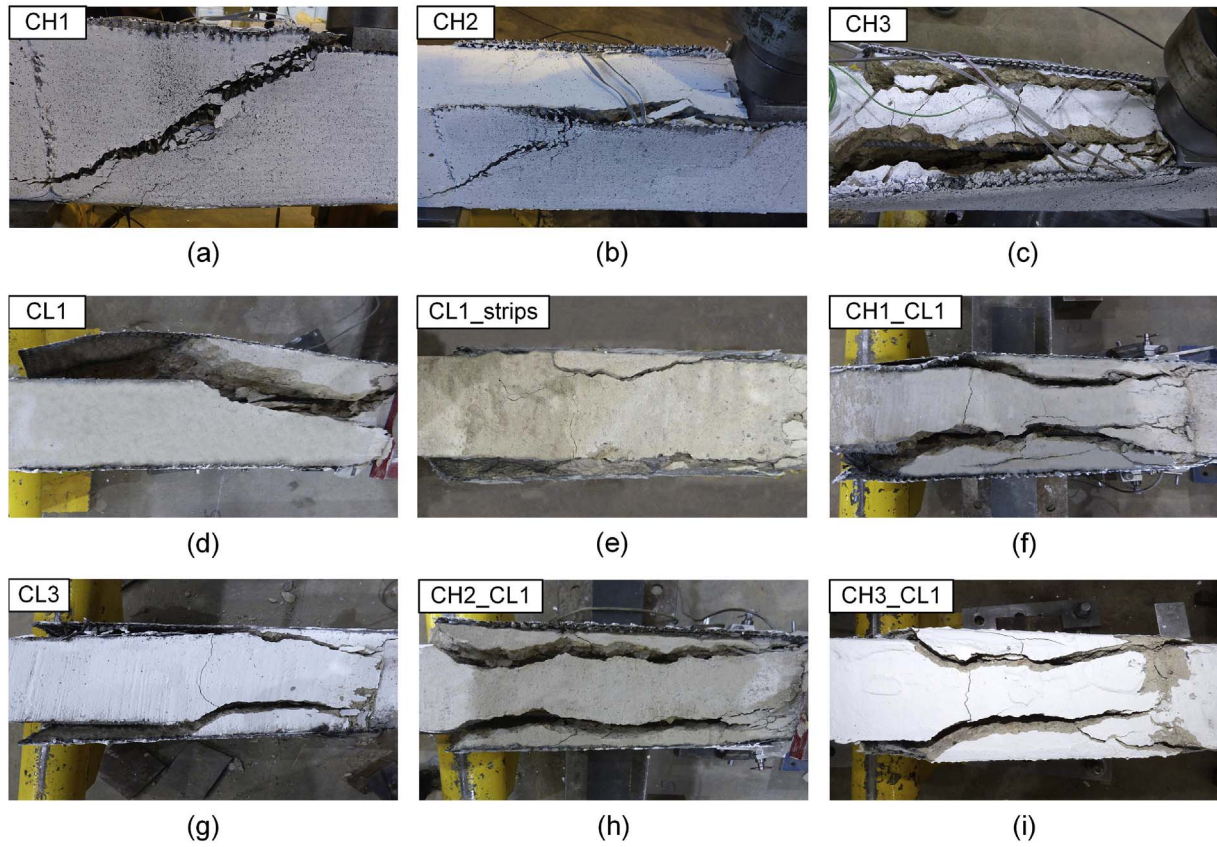


Fig. 9. Failure modes of carbon TRM-retrofitted specimens of 2.6 shear span-to-depth ratio: (a) specimen CH1 – local damage of the jacket; (b) specimen CH2 – debonding of the jacket over a large area of the shear span: peeling off of the concrete cover; (c)–(j) specimens CL1, CL1_strips, CH1_CL1, CL3, CH2_CL1, CH3_CL1 - abrupt debonding of the TRM jacket over the whole area of the shear span: peeling off of the concrete cover.

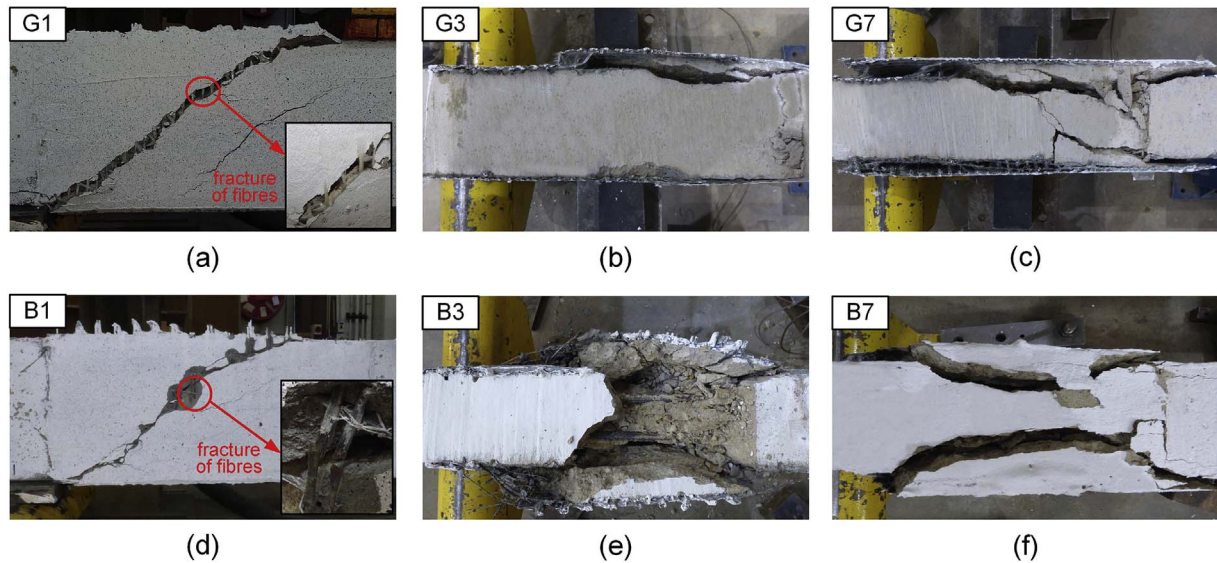


Fig. 10. Failure modes of glass and basalt TRM-retrofitted specimens of 2.6 shear span-to-depth ratio: (a) specimen G1 - fracture of glass TRM jacket; (b)–(c) specimens G3 and G7 - debonding of the glass TRM jacket over the whole area of the shear span: peeling off of the concrete cover; (d) specimen B1 - fracture of basalt TRM jacket; (e)–(f) specimens B3 and B7 - debonding of the basalt TRM jacket over the whole area of the shear span: peeling off of the concrete cover.

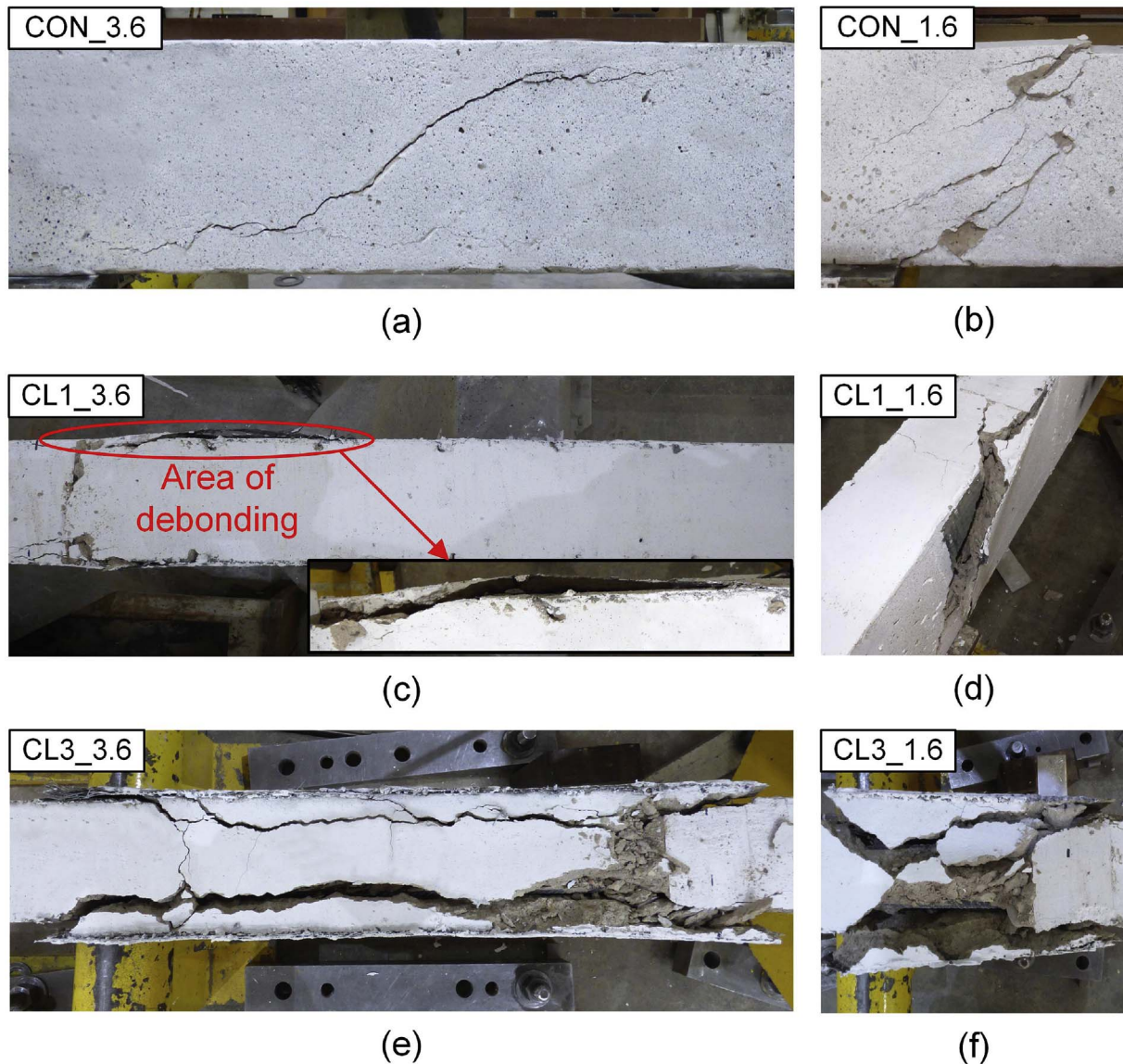


Fig. 11. Failure modes of specimens of 1.6 and 3.6 shear span-to-depth ratios: (a) specimen CON_3.6 - dominant shear crack; (b) specimen CON_1.6 - multiple shear cracks; (c) specimen CL1_3.6 - debonding of the jacket at area below the shear crack: peeling off of the concrete cover; (d) specimen CL1_1.6 - debonding of the TRM jacket over the whole area of the shear span: peeling off of the concrete cover; (e)–(f) specimens CL3_3.6 and CL3_1.6 - debonding of the TRM jacket over the whole area of the shear span: peeling off of the concrete cover.

CH1 and CL1_strips were 3.06‰ and 6.64‰, respectively. Fig. 14a–d depict field of the vertical deformations of the TRM jackets at the instant of ultimate load, obtained using DIC system. From Fig. 14a, it is evident that in specimen CH1, the TRM jacket deformed only along the main and secondary shear cracks, whereas the rest part of the jacket was not activated. On the contrary, in specimen CL1_strips (Fig. 14b), the distribution of deformations was better, indicating that the jacket was activated over a broader area due to favourable redistribution of stresses. The superior performance of the light carbon textile is possibly associated with the better fibres distribution along the shear span (denser mesh-pattern of the textile), which in turn improves the mechanical interlock between the textile reinforcement and the matrix.

Specimens CH2 and CL3 both failed due to debonding of the TRM jacket, with similar shear capacity increase (132% and 127.6%, respectively). As shown in Fig. 14c and d, in both specimens the vertical

deformations were distributed over a broad region of the shear span. Thus, the increase of external reinforcement ratio, ρ_f (through the increase of the number of layers), eliminated the effect of the textile geometry.

The results of specimens CL1, CH1, G1 and B1 shows that the performance of the heavy-carbon fibre textile was poor as its failure was associated with slippage of the vertical fibres through the mortar contrary to the rest textiles (light-carbon, glass and basalt) in which slippage of the fibres through the mortar was not observed at the load level that CH1 specimen failed. This could be attributed to the characteristics of the roving in each textile. As shown in Fig. 13a–d, the area of one roving in the direction of loading of the light-carbon, glass and basalt textile is approximately 0.5 mm², whereas the roving area in the heavy-carbon textile is almost double (0.95 mm²). As a result, in textiles with small roving area (A_{rov}), the degree of impregnation of fibres with

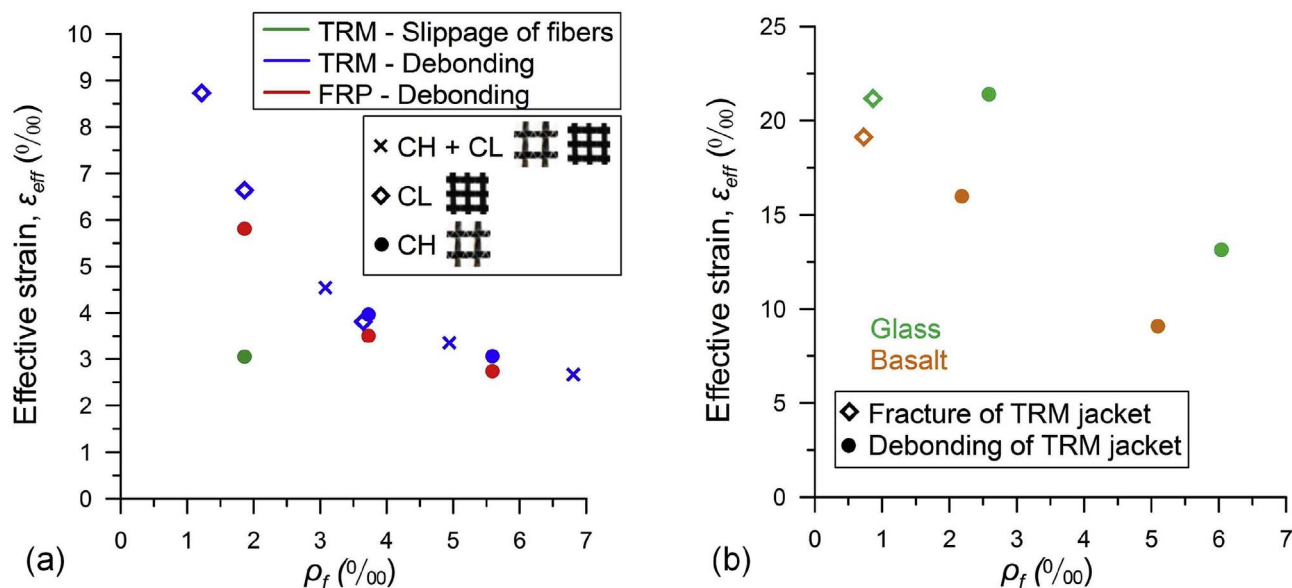


Fig. 12. Experimentally obtained effective strains versus ρ_f values and $\rho_f E_{f,TRM}$ values for specimens strengthened with carbon TRM and FRP U-jackets (a–b) and specimens strengthened with glass and basalt TRM U-jackets (c–d).

cement paste is higher, resulting in improved bond characteristics. On the other hand, textiles with bigger roving size are more prone to slippage of the fibre rovings through the matrix, unless they are coated, as in the case of the basalt textile used in this study.

4.3. Effect of shear span-to-depth ratio (a/d)

Fig. 15 illustrates the effect of the shear span-to-depth ratio (a/d) on the shear resistance of the unretrofitted specimens, $V_{R,con}$. It is well-known that increasing the a/d ratio the shear resistance decreases; this was also verified in this study, as shown in Fig. 15. This behaviour is explained through the different load-carrying mechanisms in each case. In specific, the arch action is the dominant mechanism of shear resistance in unretrofitted beams with low a/d ratio (i.e. $a/d = 1.6$, deep beams), whereas beam action (truss analogy mechanism) is developed in beams of high shear span-to-depth ratios ($a/d = 2.6$ and 3.6).

A comparison between specimens CL1.1.6, CL3.1.6, CL1, CL3, CL1.3.6 and CL3.3.6 shows that the a/d ratio had no effect on the failure mode of specimens strengthened with the same TRM jackets. All specimens failed due to debonding of the TRM jacket with peeling off of the concrete cover. In specific, when 3 TRM layers were applied in specimens of any a/d ratio, the part of concrete that peeled off from the substrate was thicker with respect to the specimens strengthened with 1

TRM layer (Fig. 11c–f). Fig. 16 presents images of the in-plane vertical deformations of the TRM jackets in beams of different shear spans, obtained through DIC measurements at the instant of peak load. In general, vertical deformations of TRM jackets with both 1 and 3 light-carbon TRM layers were distributed over a broad area of the shear span for all beams of different shear a/d ratios as a result of the good mechanical interlocking characteristics and the small roving size of the light carbon textile.

Fig. 17a illustrates the effect of the a/d ratio on the contribution of the jacket to the total shear capacity, V_f , for two different external reinforcement ratios ($\rho_f = 1.2\%$ and $\rho_f = 3.6\%$). The a/d ratio has practically no effect on the V_f values for TRM jackets regardless the external reinforcement ratio. Fig. 17b illustrates the effect of the a/d ratio on the shear capacity enhancement ($V_f/V_{R,con} \times 100\%$) for two different external reinforcement ratios ($\rho_f = 1.2\%$ and $\rho_f = 3.6\%$). The shear capacity enhancement considerably increases with a/d . This is attributed to the reduced shear resistance of the unretrofitted specimens when increasing the a/d ratio (Fig. 15).

5. Comparison between experimental results and analytical models

Based on the results of this paper and previous studies of the

Table 4
Summary of FRP-strengthened specimens results.

Specimen	ρ_f (%)	E_f (GPa)	$E_{f,FRP}$ (GPa)	Ultimate tensile strain, ϵ_{fu} (%)	Ultimate tensile strength, f_{fu} (MPa)	Peak Load (kN)	V_f (kN)	ϵ_{eff} (%)
CH1_R ^a	1.9	225	200.7	1.261	2788.4	113.4	35.3	5.81
CH2_R ^a	3.7	225	200.7	1.261	2788.4	126.2	42.6	3.51
CH3_R ^b	5.6	225	200.7	1.261	2788.4	139.0	49.9	2.74

^a Specimens included in Tetta et al. 2015 [28].

^b Specimen included in Tetta and Bournas 2016 [4].

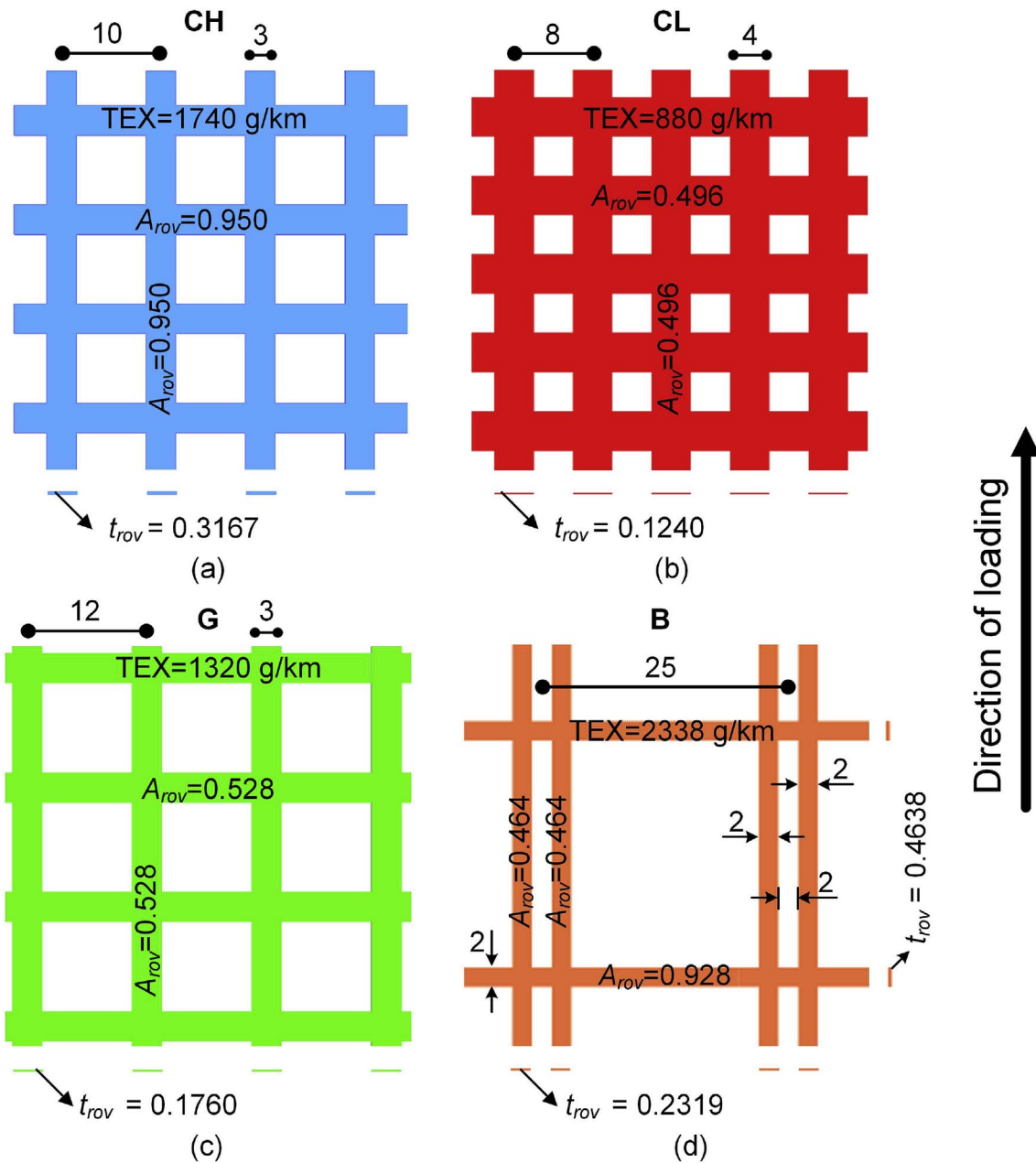


Fig. 13. Textile properties and geometry of roving in: (a) heavy carbon textile; (b) light carbon textile; (c) glass textile and (d) basalt textile.

authors, TRM jackets are as effective as FRP jackets when local damage of the TRM jackets (slippage of vertical fibres through the mortar and rupture of the outer fibres of the roving along the shear crack) is prevented and failure is attributed to debonding of the TRM jacket. Therefore, the formulas that have been developed so far for predicting the shear contribution of FRP U-jackets, V_f , to the total shear resistance of beams, could be also used for TRM jackets when failure is due to debonding. Three different models, namely those of Triantafillou and Antonopoulos (2000), [59] (provisions of *fib* 2001 [60] are based on this model), Chen and Teng (2003), [61] (the Australian guidelines provisions, CIDAR (CT) Design Proposal (2006) [62] are based on this

model) and Monti and Liotta (2007), [63] (the Italian guidelines provisions, CNR Design Proposal (2004) [64] are based on this model) were used for the prediction of V_f values for both TRM and FRP jackets. The results are presented in Table 5, and are supported by Fig. 18. The methodology to estimate the FRP or TRM contribution in shear, V_f , according to each of the aforementioned models is briefly presented in the Appendix. The modulus of elasticity of fibres, E_f (Table 1), was used in these calculations.

The comparison between the experimental and predicted V_f values is presented in Table 5 (using $\theta = 45^\circ$ and $\beta = 90^\circ$) for specimens failed due to debonding of the TRM or FRP jacket. The model of Triantafillou

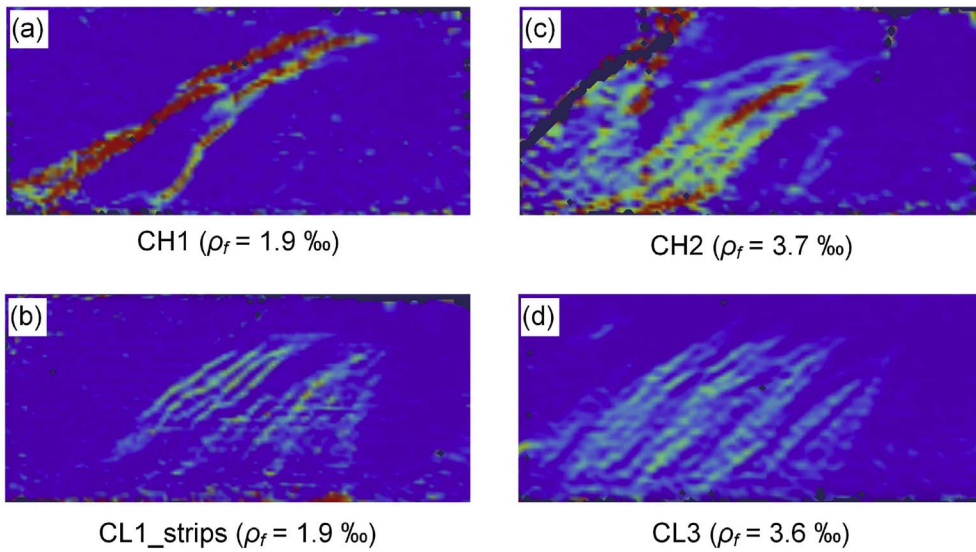


Fig. 14. Field of vertical axis deformations in the critical shear span of TRM-retrofitted specimens: (a) CH1; (b) CL1_strips; (c) CH2; (d) CL3 at the instant of peak load.

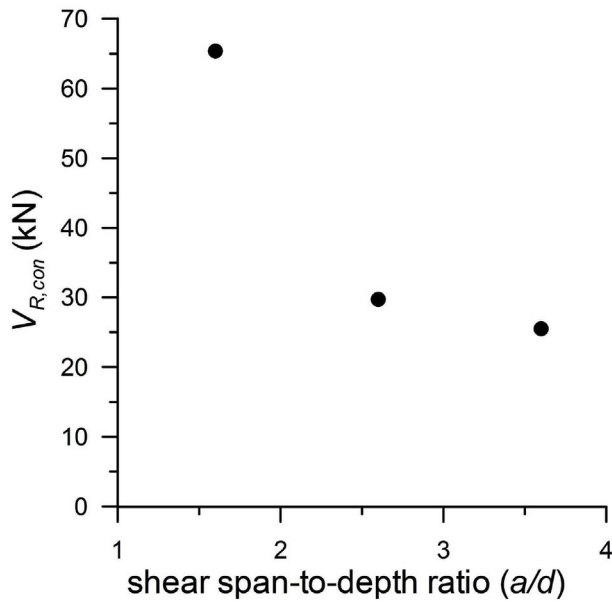


Fig. 15. Effect of shear span-to-depth ratio on the shear resistance of the control specimen.

and Antonopoulos (2000) is not applicable for specimens reinforced by either glass or basalt TRM jackets. In general, all three models underestimate the V_f values, and therefore they give conservative predictions. The models of Chen and Teng (2003) and Monti and Liotta (2007), that are applicable for glass and basalt TRM jackets, considerably underestimate the contribution of glass and basalt TRM jackets.

In particular, the model of Chen and Teng (2003) is the best in terms of average ratio of predicted to experimental peak load ($V_{f,pre}/V_{f,exp} = 0.741$); it has however a coefficient of variation (CoV) value equal to 16.9%. The model of Triantafyllou and Antonopoulos (2000) is the 2nd best among the three, with $V_{f,pre}/V_{f,exp}$ equal to 0.715 but is has the lowest CoV = 12%, whereas model of Monti and Liotta (2007) has $V_{f,pre}/V_{f,exp} = 0.598$ and CoV = 18.6%. When only the carbon fibre textiles are considered, the Chen and Teng (2003) is the best both terms of average ratio of $V_{f,pre}/V_{f,exp} = 0.801$ and CoV = 8.98%, followed by

that of Triantafyllou and Antonopoulos (2000, corresponding values as above) and that of Monti and Liotta (2007) with corresponding values of 0.648 and 9.52%, respectively.

6. Conclusions

In this paper the effectiveness of U-shaped TRM jackets for strengthening in shear rectangular concrete beams was experimentally investigated, including the following parameters: the amount of external TRM reinforcement ratio (ρ_f) using three different textile materials (carbon, glass and basalt), the textile geometry and the shear span-to-depth ratio (a/d) in RC rectangular beams strengthened in shear with U-shaped TRM jackets. For this purpose, 22 shear-deficient beams were tested under monotonic three-point loading. The primary conclusions of this paper are summarized as follows:

- Carbon TRM U-jackets are as effective as carbon FRP U-jackets in increasing the shear capacity of beams, when failure is attributed to full debonding of the jacket with part of the concrete cover attached to it.
- The experimental effective strain values, ϵ_{eff} , for carbon, glass or basalt TRM jackets are generally decreasing for increasing axial rigidity ($\rho_f E_{f,TRM}$), when failure is associated with debonding of the TRM jacket, which is in agreement with the typical behaviour of FRP jackets.
- In case of low $\rho_f E_{f,TRM}$ value, different carbon fibre textile geometries having the same $\rho_f E_{f,TRM}$ value result in different load increase and failure mode. The effect of the geometry of the textile fibre material is drastically mitigated by increasing the $\rho_f E_{f,TRM}$ value.
- The textile roving geometry affects the performance of TRM jackets in case of low axial rigidity. In particular, textiles with smaller roving area arranged in a denser pattern result in better bond characteristics between the textile and the mortar, and hence improved efficiency.
- The shear span-to-depth ratio has no effect on both the failure mode and the contribution of the jacket to the total shear resistance of the beams.

Future research could be directed towards developing a reliable design approach for the contribution of TRM jackets to the shear capacity of concrete beams.

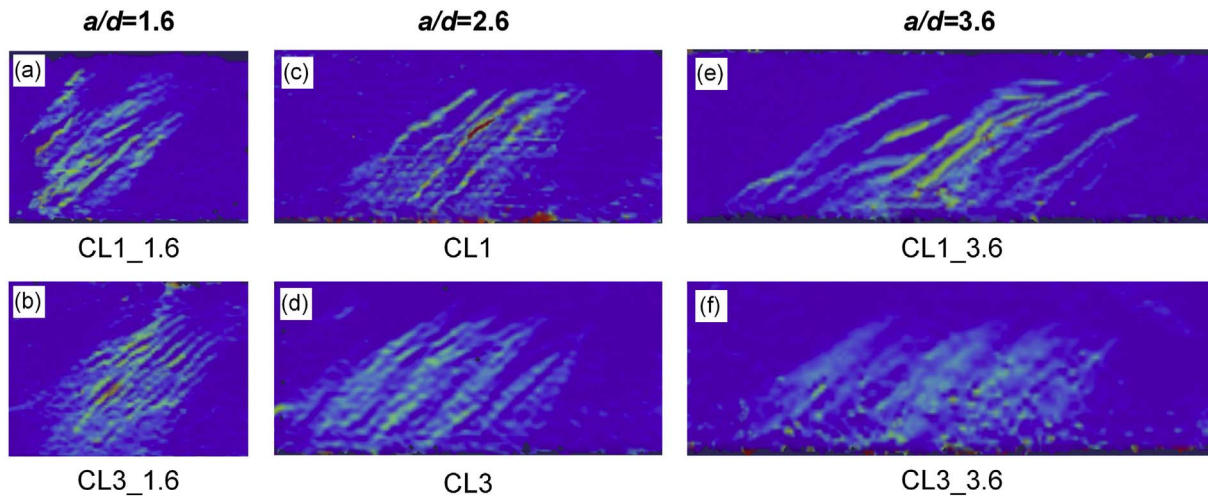


Fig. 16. Field of vertical axis deformations in the critical shear span of TRM-retrofitted specimens: (a) CL1_1.6; (b) CL3_3.6; (c) CL1; (d) CL3; (e) CL1_1.6; (f) CL3_3.6 at the instant of peak load.

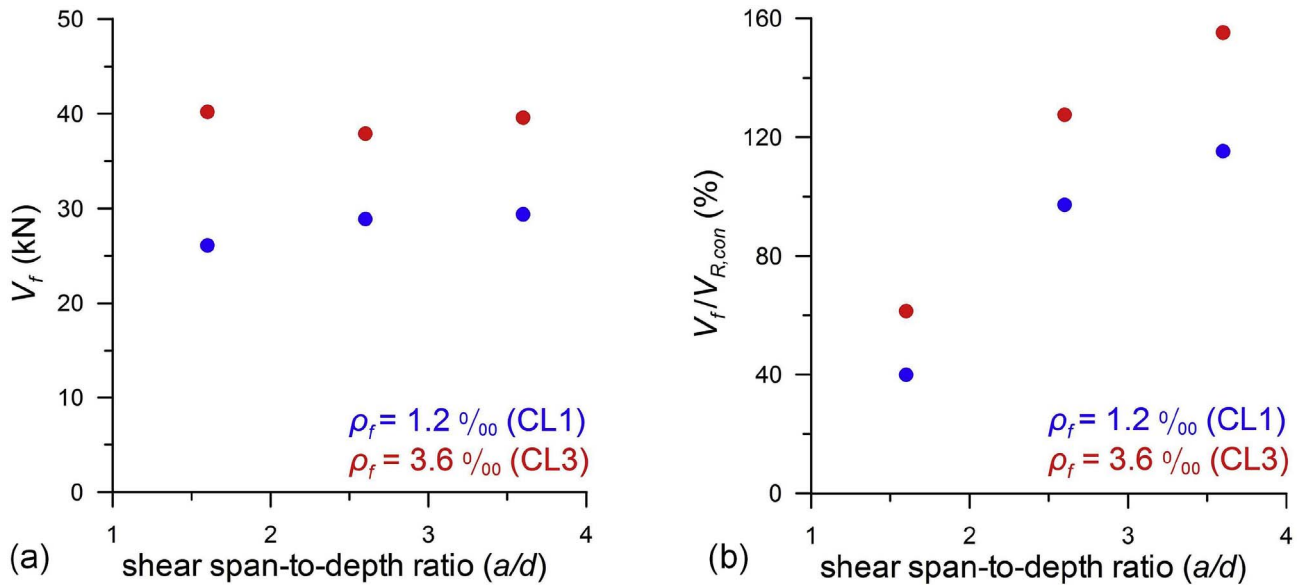


Fig. 17. Effect of shear span-to-depth ratio on: (a) the contribution of the jacket to the total shear resistance, V_f ; (b) the shear capacity enhancement, $V_f/V_{R,con}$ (%).

Table 5
Comparison between experimental and predicted V_f values.

	$V_{f,exp}$ (kN)	Analytical Results					
		Triantafyllou and Antonopoulos (2000)		Chen and Teng (2003)		Monti and Liotta (2007)	
		$V_{f,pre}$ (kN)	$V_{f,pre}/V_{f,exp}$	$V_{f,pre}$ (kN)	$V_{f,pre}/V_{f,exp}$	$V_{f,pre}$ (kN)	$V_{f,pre}/V_{f,exp}$
CL1	28.9	16.5	0.570	21.8	0.755	18.1	0.625
CL1_strips	33.7	22.1	0.655	25.2	0.748	19.5	0.578
CL1_CH1	37.6	27.5	0.731	30.5	0.811	23.6	0.628
CH2	39.2	31.9	0.814	34.5	0.881	29.9	0.762
CL3	37.9	30.1	0.793	32.8	0.866	27.3	0.720
CL1_CH2	44.4	33.9	0.763	36.0	0.811	28.0	0.630
CH3	45.4	37.4	0.824	39.0	0.860	34.7	0.763
CL1_CH3	48.5	39.0	0.804	39.7	0.819	30.9	0.637
G3	37	NA	NA	18.0	0.485	13.9	0.375
G7	53	NA	NA	25.7	0.485	19.9	0.375
B3	36.1	NA	NA	18.8	0.521	15.5	0.429

(continued on next page)

Table 5 (continued)

	$V_{f,exp}$ (kN)	Analytical Results					
		Triantafillou and Antonopoulos (2000)		Chen and Teng (2003)		Monti and Liotta (2007)	
		$V_{f,pre}$ (kN)	$V_{f,pre}/V_{f,exp}$	$V_{f,pre}$ (kN)	$V_{f,pre}/V_{f,exp}$	$V_{f,pre}$ (kN)	$V_{f,pre}/V_{f,exp}$
B7	47.9	NA	NA	27.0	0.563	22.4	0.467
CL1_1.6	26.1	16.1	0.615	21.0	0.805	16.2	0.619
CL3_1.6	40.2	29.7	0.740	32.5	0.809	25.1	0.623
CL1_3.6	29.4	16.1	0.546	21.0	0.715	16.2	0.550
CL3_3.6	39.6	29.7	0.751	32.5	0.822	25.1	0.633
CH1_R	35.3	22.5	0.636	26.4	0.747	22.5	0.638
CH2_R	42.6	31.9	0.749	34.5	0.811	29.9	0.701
CH3_R	49.9	36.3	0.727	37.9	0.760	30.5	0.611
Mean			0.715		0.741		0.598
CoV (%)			12.0		16.9		18.6
Average absolute error %			28.5		25.9		40.2
Mean for carbon fibre textiles			0.715		0.801		0.648
CoV (%) for carbon fibre textiles			12.0		5.98		9.52
Average absolute error %			28.5		19.9		35.2

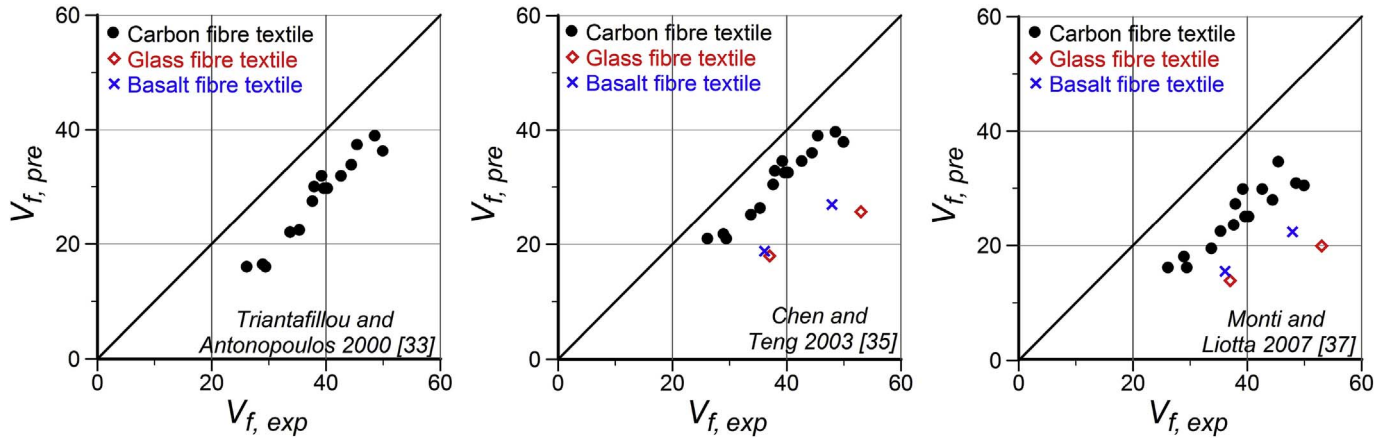


Fig. 18. Experimental versus analytical V_f values.

Acknowledgements

This work was supported by the Engineering and Physical Sciences Research Council [grant number EP/L50502X/1]. The authors wish

thank the technical staff at the University of Nottingham Tom Buss, Mike Langford, Nigel Rook, Balbir Loyla, Gary Davies, Sam Cook and Luke Bedford, the student Yuchao Shang and Dr. Saad Raouf for their assistance to the experimental work.

Appendix

V_f calculation methodology

1. Triantafillou and Antonopoulos (2000)

$$V_f = 0.9d\rho_f E_f \epsilon_{eff} b_w (\sin \beta + \cos \beta)$$

For U-shaped jackets

$$\epsilon_{eff} = \min \begin{cases} 0.17 \left(\frac{f_c^{2/3}}{\rho E_f} \right)^{0.3} \epsilon_{fu} \\ 0.65 \left(\frac{f_c^{2/3}}{\rho E_f} \right)^{0.56} 10^{-3} \end{cases}$$

2. Chen and Teng (2003)

$$V_f = 2f_{ed} t_f h_{fe} b_w (\sin \beta + \cos \beta)$$

$$h_{fe} = z_b - z_i; z_b = 0.9d - d_{fb}; z_i = d_{fi}$$

$$f_{fed} = D_f f_{fed, \max}$$

$$D_f = \begin{cases} \frac{2}{\pi \lambda} \left(\frac{1 - \cos\left(\frac{\pi \lambda}{2}\right)}{\sin\left(\frac{\pi \lambda}{2}\right)} \right), & \lambda \leq 1 \\ 1 - \frac{\pi - 2}{\pi \lambda}, & \lambda > 1 \end{cases} \quad \text{where } \lambda = L_{\max}/L_e$$

For U-shaped jackets $L_{\max} = 0.9d$

$$L_e = \sqrt{\frac{E_f t}{\sqrt{f_c}}}$$

$$f_{fed, \max} = \min \left\{ 0.427 \beta_w \beta_l \sqrt{\frac{E_f \sqrt{f_c}}{t}}, \phi_R f_{fu} \right\}$$

$$\beta_l = \begin{cases} 1, & \lambda \geq 1 \\ \sin\left(\frac{\pi \lambda}{2}\right), & \lambda < 1, \beta_w = 0.707 \text{ for continuous sheets and } \phi_R = 0.8 \end{cases}$$

3. Monti et Liotta (2007)

$$V_f = 2f_{fed} t_f 0.9d (\cot \theta + \cot \beta)$$

$$L_e = \sqrt{\frac{E_f t}{2f_{ct}}}$$

$$f_{fdd} = 0.8 \sqrt{\frac{2E_f \Gamma_{fk}}{t_f}}, \text{ where } \Gamma_{fk} = 0.03k_b \sqrt{f_c f_{ct}}, k_b = 1 \text{ for continuous sheets}$$

For U-shaped jackets $L_b = 0.9d$

$$\text{If } L_b < L_e: f_{fdd}(L_b) = f_{fdd} \frac{L_b}{L_e} \left(2 - \frac{L_b}{L_e} \right)$$

$$f_{fed} = f_{fdd}(L_b) \left(1 - \frac{L_e \sin \beta}{3 \min(0.9d, h_w)} \right)$$

Notation

A_{rov}	roving area
D_f	Stress distribution factor
E_f	Modulus of elasticity of the fibers
$E_{f,FRP}$	Modulus of elasticity of the FRP specimen
$E_{f,TRM}$	Modulus of elasticity of the cracked TRM specimen
L_b	Available bond length
L_e	Effective bond length
L_{max}	Available bond length
V_f	Contribution of strengthening to the shear capacity of the beam
V_R	Shear force in the critical span at peak load
$V_{R,con}$	Shear resistance of the control specimen
$V_{R,str}$	Shear resistance of the strengthened specimen
b_w	Width of the beam
d	Effective depth of the section
d_{fb}	Bottom end of the effective (TRM or FRP jacket)
d_{ft}	Coordinate of the top end of the effective (TRM or FRP jacket)
f_c	Compressive strength of concrete
f_{ct}	Tensile splitting strength of concrete
f_{fdd}	Design value for the FRP or TRM debonding stress
$f_{fdd}(L_b)$	Reduced design value for the FRP or TRM debonding stress
f_{fed}	Design value for the FRP or TRM effective stress
$f_{fed, \max}$	Maximum design stress in FRP or TRM
f_{fu}	Ultimate strength of TRM or FRP jacket
h_{fe}	Effective height of the bonded reinforcement
h_w	Height of T-beam's web
k_b	Covering/scale coefficient
t	Nominal thickness of the textile
t_{rov}	Roving thickness
Γ_{fk}	Specific fracture energy

β	Fibre angle direction with respect to the longitudinal axis of the beam
β_l	Bond length coefficient
β_w	Strip width coefficient
ε_{eff}	Effective strain
ε_{fu}	Ultimate tensile strain
θ	Angle between the shear crack and the axis of the beam
λ	Normalized maximum bond length
ρ_f	Geometrical reinforcement ratio of the composite material which is expressed as $2t_f/b_w$
φ_R	Reduction factor due to local stress in corners

References

- Triantafillou TC, Papanicolaou CG. Shear strengthening of reinforced concrete members with textile reinforced mortar (TRM) jackets. *Mater Struct* 2006;39(1):93–103.
- Bournas DA, Lontou PV, Papanicolaou CG, Triantafillou TC. Textile-reinforced mortar versus fiber-reinforced polymer confinement in reinforced concrete columns. *ACI Struct J* 2007;104(6).
- Carloni C, Bournas DA, Carozzi FG, D'Antino T, Fava G, Focacci F, et al. Fiber reinforced composites with cementitious (inorganic) matrix [Chapter 9]. In: Pellegrino C, Sena-Cruz J, editors. *Design procedures for the use of composites in strengthening of reinforced concrete structures – state of the art report of the RILEM TC 234-DUCS*. Springer, RILEM STAR Book Series; 2015. p. 349–91.
- Tetta ZC, Bournas DA. TRM versus FRP jacketing in shear strengthening of concrete members subjected to high temperature. *Compos Part B* 2016;106:190–205. <http://dx.doi.org/10.1016/j.compositesb.2016.09.026>.
- Raouf S, Koutas L, Bournas D. Bond between TRM versus FRP composites and concrete at high temperatures. *Compos Part B Eng* 2017;127:150–65.
- Raouf S, Bournas DA. TRM versus FRP in flexural strengthening of RC beams: behaviour at high temperatures. *Elsevier Construction and Building Materials* 2017;154:424–37.
- D'Ambrisi A, Feo L, Focacci F. Experimental analysis on bond between PBO-FRCM strengthening materials and concrete. *Compos Part B Eng* 2013;44(1):524–32.
- Raouf S, Koutas L, Bournas D. Bond between textile-reinforced mortar (TRM) and concrete substrates: experimental investigation. *Compos Part B* 2016;98:350–61. <http://dx.doi.org/10.1016/j.compositesb.2016.05.041>.
- Jesse F, Weiland S, Curbach M. Flexural strengthening of RC structures with textile-reinforced concrete. *American Concrete Institute*; 2008. p. 49–58. Special Publication 250.
- Sneed LH, Verre S, Carloni C, Ombres L. Flexural behaviour of RC beams strengthened with steel-FRCM composite. *Eng Struct* 2017;127:686–99.
- Raouf S, Koutas L, Bournas D. Textile-reinforced mortar (TRM) versus fibre-reinforced polymers (FRP) in flexural strengthening of RC beams. *Constr Build Mater* 2017;151:279–91.
- D'Ambrisi A, Focacci F. Flexural strengthening of RC beams with cement based composites. *J Comp Constr* 2011. [http://dx.doi.org/10.1061/\(ASCE\)CC.1943-5614.0000218](http://dx.doi.org/10.1061/(ASCE)CC.1943-5614.0000218), 707–720.
- Elsanadedy HM, Almusallam TH, Alsayed SH, Al-Salloum YA. Flexural strengthening of RC beams using textile reinforced mortar—Experimental and numerical study. *J Comp Struct* 2013;97:40–5.
- Koutas LN, Bournas DA. Flexural strengthening of two-way RC slabs with textile-reinforced mortar: experimental investigation and design equations. *J Compos Constr* 2016. [http://dx.doi.org/10.1061/\(ASCE\)CC.1943-5614.0000713](http://dx.doi.org/10.1061/(ASCE)CC.1943-5614.0000713).
- Alabdulhady MY, Sneed LH, Carloni C. Torsional behaviour of RC beams strengthened with PBO-FRCM composite—An experimental study. *Eng Struct* 2017;136:393–405.
- Bournas DA, Triantafillou TC, Zygouris K, Stavropoulos F. Textile-reinforced mortar versus FRP Jacketing in seismic retrofitting of RC columns with continuous or Lap-spliced deformed bars. *J Comp Constr* 2009;13(5):360–71.
- Bournas DA, Triantafillou TC. Bond strength of lap-spliced bars in concrete confined with composite jackets. *J Comp Constr* 2011;15(2):156–67.
- Bournas DA, Triantafillou TC. Bar buckling in RC columns confined with composite materials. *J Comp Constr* 2011;15(3):393–403.
- Bournas DA, Triantafillou TC. Biaxial bending of reinforced concrete columns strengthened with externally applied reinforcement in combination with confinement. *ACI Struct J* 2013;110(2):193.
- El-Maaddawy T, El Refai A. Innovative repair of severely corroded T-beams using fabric-reinforced cementitious matrix. *J Compos Constr* 2015;20(3). 04015073.
- Papanicolaou CG, Triantafillou TC, Lekka M. Externally bonded grids as strengthening and seismic retrofitting materials of masonry panels. *Constr Build Mater* 2011;25(2):504–14.
- Harajli M, El Khatib H, San-Jose J. Static and cyclic out-of-plane response of masonry walls strengthened using textile-mortar system. *J Mater. Civ Eng* 2010;22(11):1171–80.
- Koutas L. and Bournas D.A. Out-of-Plane Strengthening of Masonry-Infilled RC Frames with Textile-Reinforced Mortar Jackets. *Elsevier Construction and Building Materials*, 2018; submitted.
- Ombres L. Confinement effectiveness in eccentrically loaded masonry columns strengthened by fiber reinforced cementitious matrix (FRCM) jackets. *Key Eng Mater* 2015;624:551–8.
- Koutas LN, Bousias SN, Triantafillou TC. Seismic strengthening of masonry-infilled RC frames with TRM: experimental study. *J Comp Constr* 2015;19(2). [http://dx.doi.org/10.1061/\(ASCE\)CC.1943-5614.0000507](http://dx.doi.org/10.1061/(ASCE)CC.1943-5614.0000507). 04014048.
- Triantafillou TC, Karlos K, Kefalou K, Argyropoulou E. An innovative structural and energy retrofitting system for URM walls using textile reinforced mortars combined with thermal insulation: mechanical and fire behaviour. *Constr Build Mater* 2017;133:1–13.
- Bournas DA. Strengthening of existing structures: selected case studies. In: Triantafillou TC, editor. *Textile fibre composites in civil engineering* Elsevier, Woodhead Publishing Limited; 2016. p. 389–411. <http://dx.doi.org/10.1016/B978-1-78242-446-8.00018-5>. Ch. 17.
- Carabba L, Santandrea M, Carloni C, Manzi S, Bionozzi MC. Steel fiber reinforced geopolymer matrix (S-FRGM) composites applied to reinforced concrete structures for strengthening applications: a preliminary study. *Compos Part B* 2017;128:83–90.
- Valvona F, Toti J, Gattulli V, Potenza F. Effective seismic strengthening and monitoring of a masonry vault by using glass fiber reinforced cementitious matrix with embedded fiber bragg grating sensors. *Compos Part B* 2017;113:355–70.
- Donnini J, Basalo FDC, Corinaldesi V, Lancioni G, Nanni A. Fabric-reinforced cementitious matrix behavior at high-temperature: experimental and numerical results. *Compos Part B* 2017;108:108–21.
- Bilotta A, Ceroni F, Lignola GP, Protà A. Use of DIC technique for investigating the behaviour of FRCM materials for strengthening masonry elements. *Compos Part B* 2017;129:251–70.
- Caggegi C, Carozzi FG, De Santis S, Fabbrocio F, Focacci F, Lanoye E, et al. Experimental analysis on tensile and bond properties of PBO and aramid fabric reinforced cementitious matrix for strengthening masonry structures. *Compos Part B* 2017;127:175–95.
- Caggegi C, Lanoye E, Djama K, Bassil A, Gabor A. Tensile behaviour of a basalt TRM strengthening system: influence of mortar and reinforcing textile ratios. *Compos Part B* 2017;130:90–102.
- Carozzi FG, Bellini A, D'Antino T, de Felice G, Focacci F, Hojdis L, et al. Experimental investigation of tensile and bond properties of Carbon-FRCM composites for strengthening masonry elements. *Compos Part B* 2017;128:100–19.
- De Santis S, Carozzi FG, de Felice G, Poggi C. Test methods for textile reinforced mortar systems. *Compos Part B* 2017;127:121–32.
- Leone M, Aiello MA, Balsamo A, Carozzi FG, Ceroni F, Corradi M, et al. Glass fabric reinforced cementitious matrix: tensile properties and bond performance on masonry substrate. *Compos Part B* 2017:196–214.
- Trapko T, Musiał M. PBO mesh mobilization via different ways of anchoring PBO-FRCM reinforcements. *Compos Part B* 2017;118:67–74.
- Lignola GP, Caggegi C, Ceroni F, De Santis S, Krajewski P, Lourenço PB, et al. Performance assessment of basalt FRCM for retrofit applications on masonry. *Compos Part B* 2017;128:1–18.
- Marcari G, Basili M, Vestroni F. Experimental investigation of tuff masonry panels reinforced with surface bonded basalt textile-reinforced mortar. *Compos Part B* 2017;108:131–42.
- D'Antino T, Papanicolaou C. Mechanical characterization of textile reinforced inorganic-matrix composites. *Compos Part B* 2017;127:78–91.
- Nobili A, Signorini C. On the effect of curing time and environmental exposure on impregnated Carbon Fabric Reinforced Cementitious Matrix (CFRCM) composite with design considerations. *Compos Part B* 2017;112:300–13.
- Al-Salloum YA, Elsanadedy HM, Alsayed SH, Iqbal RA. Experimental and numerical study for the shear strengthening of reinforced concrete beams using textile-reinforced mortar. *J Compos Constr* 2012;16(1):74–90.
- Contamine R, Si Larbi A, Hamelin P. Identifying the contributing mechanisms of textile reinforced concrete (TRC) in the case of shear repairing damaged and reinforced concrete beams. *Eng Struct* 2013;46:447–58.
- Brückner A, Ortlepp R, Curbach M. Anchoring of shear strengthening for T-beams made of textile reinforced concrete (TRC). *Mater Struct* 2008;41(2):407–18.
- Azam R, Soudki K. FRCM strengthening of shear-critical RC beams. *J Comp Constr* 2014;18(5). [http://dx.doi.org/10.1061/\(ASCE\)CC.1943-5614.0000464](http://dx.doi.org/10.1061/(ASCE)CC.1943-5614.0000464). 04014012.
- Tzoura E, Triantafillou TC. Shear strengthening of reinforced concrete T-beams under cyclic loading with TRM or FRP jackets. *Mater Struct* 2016;49(1):17–28. <http://dx.doi.org/10.1617/s11527-014-0470-9>.
- Baggio D, Soudki K, Noël M. Strengthening of shear critical RC beams with various FRP systems. *Constr Build Mater* 2014;66:634–44.
- Tetta ZC, Koutas LN, Bournas DA. Textile-reinforced mortar (TRM) versus fiber-reinforced polymers (FRP) in shear strengthening of concrete beams. *Compos Part B* 2015;77:338–48. <http://dx.doi.org/10.1016/j.compositesb.2015.03.055>.
- Loreto G, Babeiadarabad S, Lardini L, Nanni A. RC beams shear-strengthened with

- fabric-reinforced-cementitious-matrix (FRCM) composite. *Int J Adv Struct Eng (IJASE)* 2015;1–12.
- [50] Ombres L. Structural performances of reinforced concrete beams strengthened in shear with a cement based fiber composite material. *Comp Struct* 2015;122:316–29.
- [51] Trapko T, Urbańska D, Kamiński M. Shear strengthening of reinforced concrete beams with PBO-FRCM composites. *Compos Part B* 2015;80:63–72.
- [52] Tetta ZC, Koutas LN, Bournas DA. Shear strengthening of full-scale RC T-beams using textile-reinforced mortar and textile-based anchors. *Compos Part B* 2016;95:225–39. <http://dx.doi.org/10.1016/j.compositesb.2016.03.076>.
- [53] Awani O, El-Maaddawy T, El Refai A. Numerical simulation and experimental testing of concrete beams strengthened in shear with fabric-reinforced cementitious matrix. *J Comp Constr* 2016. [http://dx.doi.org/10.1061/\(ASCE\)CC.1943-5614.0000711](http://dx.doi.org/10.1061/(ASCE)CC.1943-5614.0000711).
- [54] 1015-11 EN. Methods of test for mortar for masonry – Part 11: determination of flexural and compressive strength of hardened mortar. Brussels: Comité Européen de Normalisation; 1993.
- [55] Pellegrino C, Vasic M. Assessment of design procedures for the use of externally bonded FRP composites in shear strengthening of reinforced concrete beams. *Compos Part B* 2013;45(1):727–41.
- [56] Rousakis T, Saridaki M, Mavrothalassitou S, Hui D. Utilization of hybrid approach towards advanced database of concrete beams strengthened in shear with FRPs. *Compos Part B* 2016;85:315–35.
- [57] Rousakis T. Hybrid confinement of concrete by FRP sheets and fiber ropes under cyclic axial compressive loading. *ASCE J Compos Constr* 2013;17(5):732–43.
- [58] Rousakis T. Reusable and recyclable nonbonded composite tapes and ropes for concrete columns confinement. *Compos Part B Eng* 2016;103:15–22. 15 October 2016.
- [59] Triantafyllou TC, Antonopoulos CP. Design of concrete flexural members strengthened in shear with FRP. *J Comp Constr* 2000;4(4):198–205.
- [60] Fédération Internationale du Béton (fib). Bulletin 14 – externally bonded FRP reinforcement for RC structures 2001. TaskGroup 9.3 Technical Report.
- [61] Chen JF, Teng JG. Shear capacity of FRP-strengthened RC beams: FRP debonding. *Constr Build Mat* 2003;17(1):27–41.
- [62] CIDAR. Design guideline for RC structures retrofitted with FRP and metal plates: beams and slabs Draft 3 – Submitted to Standards Australia University of Adelaide; 2006.
- [63] Monti G, Liotta MA. Tests and design equations for FRP-strengthening in shear. *Constr Build Mater* 2007;21(4):799–809.
- [64] CNR-DT 200. Guide for the design and construction of externally bonded FRP systems for strengthening existing structures. Italy: National Research Council; 2004.